

Simulation of the hydration kinetics and elastic moduli of cement mortars by microstructural modelling

Luca Valentini^{a,b,*}, Matteo Parisatto^{b,c}, Vincenzo Russo^a, Giorgio Ferrari^a, Jeffrey W. Bullard^d, Ross J. Angel^b, Maria C. Dalconi^{b,c}, Gilberto Artioli^{b,c}

^a*R&D Department, Mapei SpA, Via Cafiero 22, 20158 Milan, Italy*

^b*Department of Geosciences, University of Padua, via Gradenigo 6, 35131 Padua, Italy*

^c*CIRCe Inter-Departmental Research Center for the Study of Cement Materials and Hydraulic Binders, via Gradenigo 6, 35131 Padua, Italy*

^d*Materials and Structural Systems Division, National Institute of Standards and Technology, Gaithersburg, MD, USA*

Abstract

The ability of the VCCTL microstructural model to predict the hydration kinetics and elastic moduli of cement materials was tested by coupling a series of computer simulations and laboratory experiments, using different cements. The novel aspects of this study included the fact that the simulated hydration kinetics were benchmarked using real-time measurements of the early-age phase composition during hydration by in-situ X-ray diffraction. Elastic moduli are measured both by strain gauges (static approach) and by P-wave propagation (dynamic approach). Compressive strengths were measured by loading mortar prisms until rupture. Virtual samples were generated by VCCTL, using particle size distribution and phase composition as input. The hydration kinetics and elastic moduli were simulated and the numerical results were compared with the experimental observations. The compressive strength of the virtual mortars were obtained from the elastic moduli, using a power-law relation. Experimentally measured and simulated time-dependence of the major cement clinker phases and hydration product

*corresponding author

Email addresses: luca.valentini@unipd.it (Luca Valentini), matteo.parisatto@unipd.it (Matteo Parisatto), hpss.lab@mapei.it (Vincenzo Russo), g.ferrari@mapei.it (Giorgio Ferrari), bullard@nist.gov (Jeffrey W. Bullard), rossjohnangel@gmail.com (Ross J. Angel), mariachiara.dalconi@unipd.it (Maria C. Dalconi), gilberto.artioli@unipd.it (Gilberto Artioli)

phases typically agreed to within 5 %. Also, refinement of the input values of the intrinsic elastic moduli of the various phases enabled predictions of effective moduli, at different ages and different water-to-cement mass ratios, that are within the 10 % uncertainty in the measured values. These results suggest that the VCCTL model can be successfully used as a predictive tool, which can reproduce the early age hydration kinetics, elastic moduli and mechanical strength of cement-based materials, using different mix designs.

Keywords: cement hydration, computer modeling, mortar, elastic properties, strength

1. Introduction

In recent years, ever-improving computational resources have facilitated the study of the 3D microstructure of cementitious materials and its relationship with the physical properties, based on computer models that generate virtual materials and accurately simulate the mechanisms of microstructural development. An integrated approach that encompasses both measurement and modeling is fundamental to understanding experimental observations and to developing an advanced design of cement-based materials.

In this study, we test the capabilities of the Virtual Cement and Concrete Testing Laboratory (VCCTL) models [1, 2, 3] developed at the National Institute of Standards and Technology (NIST) to predict the hydration kinetics, elastic properties, and compressive strength of concrete binder materials. Similar validation studies have been published previously, but they have mostly focused on theoretical aspects of modelling the development of cement paste physical properties [4, 5, 6, 7] and used indirect measurements of the hydration kinetics, based on the measurement of the degree of hydration [5, 6], or empirical relations [4, 8] rather than the measured variation of the phases present in the system, to calibrate the numerical results. In this work, we attempt to test the potential of VCCTL on mortar samples, as a predictive tool that can integrate experimental determinations for practical applications. For practical purposes, the comparison of simulated with measured variations of physical properties must be based on physical time rather than on the degree of hydration, which would require additional measurements and additional sources of error. To achieve these aims, we focussed on the following aspects:

1. The accuracy of the simulated kinetics is benchmarked using in-situ X-ray diffraction experiments coupled with Rietveld refinement, which returns the actual time-dependent phase composition of the hydrating cement paste. Both simulation and experiments were performed on three different cements, prepared at a different water-to-cement mass ratios (w/c) and cured at different temperatures.
2. A detailed evaluation of the intrinsic elastic properties relative to the individual phases is performed, based on a review of recent literature data. Particular focus is given to the elastic moduli of the C-S-H phase, whose values are extrapolated by a quantitative method.
3. Both static and dynamic elastic moduli, in addition to compressive strength, are measured for mortars with different composition and w/c, to establish the most appropriate method of measurement to be used for comparing actual and predicted properties.
4. A general working relationship between elastic moduli and strength is defined, based on different cements and w/c.

2. Materials and experimental methods

The starting materials used in this work were an ordinary CEM I 52.5R Portland cement and a limestone CEM II/A-LL 42.5R Portland cement ¹ (hereafter C1 and C2). A third mix was obtained from a CEM I 52.5R cement blended with 5% and 10% by mass of silica fume (hereafter C3), and used to validate the relationship between elastic moduli and compressive strength. The solid oxide composition and mineralogical phase composition, as measured by X-ray fluorescence and X-ray diffraction, respectively, are shown in Tables 1 and 2. The particle size distributions, measured by laser scattering, are displayed in Figure 1. The aggregate used for the mortar samples is a CEN normalized siliceous sand, having a mean solid density of 2620 kg/m³, a bulk modulus of 33.2 GPa and a shear modulus of 24.5 GPa.

Mortar samples were used as reference test materials to study the accuracy of the computer model in predicting compressive strength and elastic moduli. The mortars were prepared by mixing 0.9 kg of cement with 2.7 kg of sand. The adopted mixing procedure and curing conditions were based on the EN 196-1 standard [10]. Three different w/c ratios were selected for the C2 (0.5, 0.55 and 0.6), two for C1 (0.5 and 0.6) and one for C3 (0.5).

¹Cement types are defined based on the EN 197-1 standard [9].

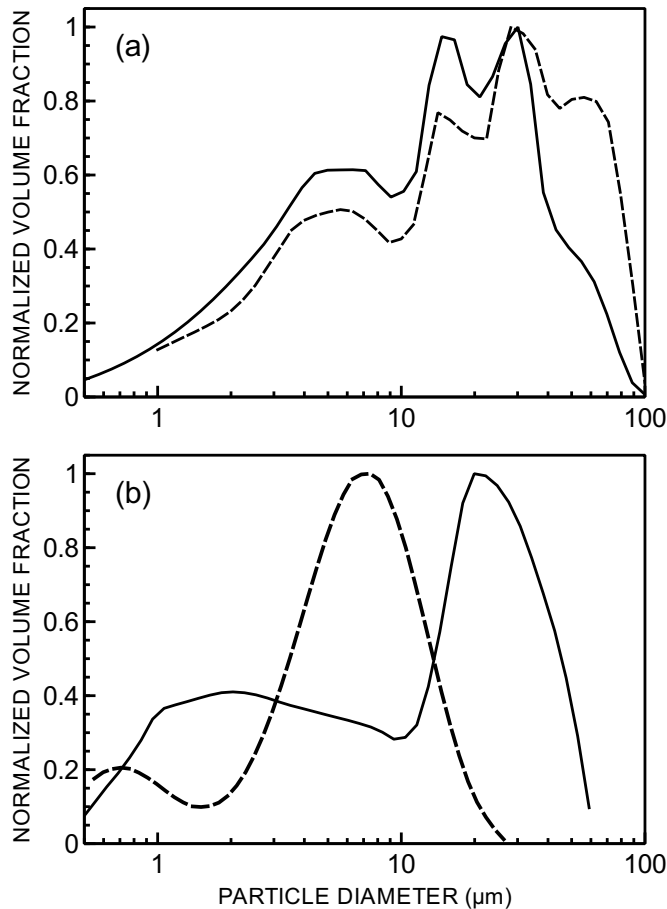


Figure 1: Particle size distributions for the starting materials used in the study, displayed as probability density functions. (a) C1 (solid line) and C2 (dashed line); (b) C3 (solid line) and silica fume (dashed line) Each curve is the average of three measurements, with the variability about the same as the thickness of the line.

Table 1: Oxide chemical composition measured by XRF for the cements and silica fume studied. The uncertainty associated with the measurements is less than 1 %.

cement	SiO ₂	Al ₂ O ₃	Fe ₂ O ₃	MgO	CaO	Na ₂ O	K ₂ O	SO ₃	Sum
C1	19.4	5.5	1.8	3.1	60.8	1.2	0.4	3.2	95.3
C2	20.6	4.6	2.5	1.7	65.5	-	0.7	2.5	98.1
C3	21.5	4.6	2.2	2.7	65.1	0.1	0.7	2.0	97.0
Silica fume	94.7	0.5	1.7	0.7	0.3	0.5	0.7	-	99.1

Table 2: Mineral phase proportions measured by XRD for the cements studied. Numbers in parentheses are estimated uncertainty expressed as per cent by mass, based on the results of [11].

Phase	C1 (mass %)	C2 (mass %)	C3 (mass %)
Alite	60 (5)	58 (5)	58 (5)
Belite	19 (5)	13 (3)	17 (4)
Aluminate	8 (3)	8 (3)	9 (3)
Ferrite	4 (1)	7 (2)	3(1)
Gypsum	2	1	1
Bassanite	3	1	4
Arcanite	1	–	–
Calcite	–	12	–
Periclase	2	–	2

2.1. Compressive strength and elastic moduli measurements

Measurements of the mechanical and elastic properties were performed on mortar prisms with standard dimensions 40 mm × 40 mm × 160 mm. Compressive strength and elastic moduli measurements were performed at 1 d, 7 d, and 28 d of hydration for C1 and C2. For C3, compressive strengths were measured at 28 d 60 d of hydration, for additions of 5% and 10% by mass of silica fume.

The axial compressive strengths were measured by loading the mortar prisms between plates with dimensions 40 mm × 40 mm until rupture, as prescribed by the EN 196-1 standard [10].

The Young’s modulus of each mortar prism was measured both by a dynamic and a static method. The dynamic measurements were made by a non-invasive method using the propagation of compressional waves (P-waves) through the sample. The dynamic Young’s modulus E_d is calculated from the measured P-wave velocity according to

$$E_d = \frac{(1 + \nu)(1 - 2\nu)}{1 - \nu} \rho V_P^2 \quad (1)$$

where ν and ρ are the measured Poisson’s ratio and density of the material, respectively. The Poisson’s ratio of each mortar prism was measured by equipping the prisms with three strain gauges. Two gauges were placed on opposite faces in order to measure the extent of the compression, parallel

to the direction of the applied load, whereas the third gauge was placed at right angles, in order to measure the transverse extension. Values of the Poisson ratio of 0.20 and 0.18 were obtained at 7 d and 28 d, respectively, and a value of 0.20 was assumed at 1 day. Static measurements of Young’s modulus, performed following the UNI 6556 standard [12], were based on stress–strain curves using three strain gauges, each placed along one of the faces parallel to the major axis of the mortar prisms.

2.2. *In-situ X-ray powder diffraction*

Early age hydration kinetics were studied by in-situ X-ray diffraction (XRD) performed on cement pastes obtained by mixing C1 and C2 with deionised water at $w/c = 0.5$ and 0.6 , respectively. The samples were prepared using an orbital shaker, with a mixing time of one minute, placed in a sample holder having a diameter of 35 mm and covered with an X-ray transparent foil. XRD patterns were acquired using a diffractometer in Bragg-Brentano geometry, equipped with a Cu-anode X-ray tube. The measurements were performed in-situ, at time intervals of 20 min, up to about 20 h after the beginning of hydration. Isothermal conditions of 25 °C and 23 °C were used for C1 and C2, respectively.

The volume fraction of each crystalline phase was determined by Rietveld full-profile fitting analysis. The fundamental parameters approach was applied to simulate the instrumental contribution to line broadening and asymmetry [13]. The instrumental parameter values were determined by refining a pattern of the standard reference material LaB_6 (NIST SRM 660a). Structural models for crystalline phases were taken from the Inorganic Crystal Structure Database [14] and the background contribution of the film was described with the peak-phase approach [15]. Lattice parameters and Lorentzian peak broadening of alite, belite, ferrite, tricalcium aluminate and gypsum were determined by Rietveld refinement of dry cement powder. These values were kept fixed during refinement of the products of hydration. A preferred orientation correction was applied for gypsum and portlandite phases. The volume fractions of C–S–H and capillary water were inferred from mass balance calculations, following the approach described in [16].

3. Computational model

3.1. Overview of the VCCTL model

VCCTL was used to simulate the development of mechanical properties for virtual models of the materials described in Section 2. VCCTL is a suite of integrated, microstructure-based computer models for creating virtual 3D cement paste microstructures, for simulating the hydration of those microstructures under a variety of curing conditions, and for calculating the time-dependent mechanical and transport properties of concrete materials made using the paste as the binder. The phase composition, w/c ratio and particle size distribution of the cement, as well as the amount, grading and physical properties of the aggregate (*i.e.*, density, bulk and shear moduli) are supplied as input by the user. Spherical harmonics are used to describe the shape of the clinker particles [17, 18], and autocorrelation functions are used to spatially distribute the individual clinker phases within the particles [19], thereby producing multiphase clinker particles with realistic distributions in size and shape. The microstructure is mapped onto a regular cubic lattice of voxels with a linear resolution of $1\ \mu\text{m}/\text{voxel}$. The dimensions of the computational domain are between $100\ \mu\text{m}$ and $200\ \mu\text{m}$, and periodic boundary conditions are used in each dimension.

VCCTL simulates microstructure development during cement paste hydration using an agent-based model that is based on a set of probabilistic rules to mimic the dissolution, diffusion, and precipitation of the phases present in the system [4]. The number of iterations performed by the hydration model are converted into physical time by calculating the heat release based on the simulated phase composition at each time step and on the enthalpy of dissolution–precipitation of the single phases. The conversion to physical time is performed by calibrating the predicted heat curve to experimental curves obtained by isothermal calorimetry. The output is represented by a 3D digital microstructure, in which each voxel is assigned a unique index corresponding to a given cement phase (Figure 2).

The simulated microstructure is used as input for the calculation of the linear elastic moduli of the material. This is achieved by a multi-scale approach. At the smaller length scale, the linear elastic moduli of the cement paste are calculated by a finite element (FE) model that assigns a trilinear cubic mesh element to each voxel of the digital microstructure and enforces periodic boundary conditions to the computational domain. The phases assigned to each voxel are assumed to be elastically isotropic. The effective

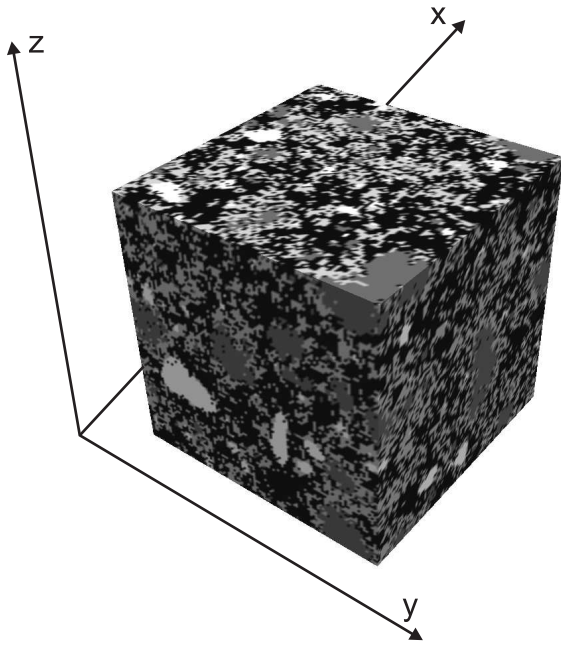


Figure 2: VCCTL-generated microstructure for a limestone cement paste, with $w/c = 0.5$, at two days of hydration. Black = pores; dark gray = unhydrated clinker; light gray = hydration products; white = calcite.

elastic moduli of the paste are then calculated by minimizing the total elastic energy in response to an applied displacement [20]. The mesh elements are elastically connected at their corners, so even incidental contact of two unhydrated cement grains produces an artificial elastic connection and leads to significant overestimates of elastic moduli at early ages when such particle-particle contacts are common. This is an artifact of the digitized representation of the microstructure that becomes less pronounced at later ages once the hydrating cement particles are covered with hydration products. Here, we reduce the influence of this artifact by searching the microstructure for incidental grain contacts and manually severing them by randomly selecting one of the two elements defining the contact and replacing its solid phase with water. This procedure reduces the volume fraction of solid clinker phases by $\sim 1\%$ at early ages.

At the scale of the mortar, the effective elastic moduli of the composite material are computed from differential effective medium theory, which treats the cement paste as an elastically homogeneous matrix. The calculation proceeds iteratively; in each iteration a small number of aggregate particles are embedded in the matrix and the dilute limit is used to calculate the composite moduli. This composite is then homogenized into a new matrix with those properties in the next iteration. The process is repeated until the target volume fraction of aggregate particles is reached. Full details of the procedure are available elsewhere [1, 21].

Elastic moduli are rarely measured for industrial samples, but the compressive strength is frequently measured as an indicator of mechanical integrity and of anticipated structural performance. However, fundamental calculation of compressive strength of a random composite material is an especially difficult task because it depends on subcritical crack formation, growth, and coalescence. As an empirical alternative, we use a power-law relation between compressive strength and Young’s modulus of the concrete or mortar similar to that proposed by Neville [22]. We stress that, because of its empirical nature, any such relation must be calibrated to experimental data. For this purpose, we measured both the dynamic Young’s modulus and the compressive strength at different hydration times for mortars using either C1 or C2 as the binder. In addition, we also incorporated into the calibration similar measurements reported recently by Siam Research and Innovation Co., Ltd. (SRI) [8]. The data and calibration for relating strength to Young’s modulus are reported in Section 4.2.

3.2. Elastic properties of the individual cement phases

Given the elastically anisotropic nature of the individual cement phases, the elastic moduli of the multi-phase cement materials should ideally be computed from the full elastic tensors of the single phases. However, full elastic tensors have been calculated only for a few of the phases found in cement materials. Moreover, the use of full elastic tensors requires assumptions on the orientation of the phases present in the microstructure, and is computationally intensive, so VCCTL accepts isotropic averages of the full elastic tensors as input for the FE computation. However, such isotropic averages cannot be unequivocally defined and depend on the way the phases mechanically interact with each other. Lower and upper bounds for polycrystals, known as Reuss and Voigt bounds [23], can be defined for each phase. The difference between the Reuss and Voigt bounds increases with the degree of elastic anisotropy [23]. Here, we compare the results of experimental measurements with numerical calculation of the elastic moduli, obtained using Voigt-Reuss-Hill averages (*i.e.*, average between Reuss and Voigt moduli, hereafter VRH). VRH moduli are used here because: a) the clinker phases, as well as ettringite, are nearly elastically isotropic and there is no significant difference between the Reuss and Voigt averages; b) only VRH values are reported in the published literature for C–S–H. Recommended VRH averages for phases relevant to cement materials are summarized in Table 3.

The values of the elastic moduli for the main clinker phases alite (C_3S), belite (C_2S), and aluminate (C_3A) were inferred from a combination of measurements obtained by resonant ultrasonic spectroscopy, nano-indentation [24] and single-crystal compression [25, 26] with simulations performed using density functional theory and interatomic potentials [27, 28, 29]. The data for calcite [30], ettringite [31] and portlandite [32] were measured by Brillouin spectroscopy performed on well-characterised materials. The values for gypsum and anhydrite were obtained by ultrasonic measurements [33] and mechanical compression tests [34] performed on single crystals, respectively. The values for bassanite were estimated from a powder diffraction compressional study [35]. Elasticity data for monosulfoaluminate phases are not available in the literature. Values of the elastic moduli equivalent to those of portlandite were assigned based on the similarity between the two crystal structures [36].

Published experimental data on the elasticity of C–S–H are scarce, due to the absence of long range order in this phase. This is unfortunate in terms of modelling the elastic and mechanical properties of cement materials, since C–S–H is the dominant phase for the development of such properties in hy-

Table 3: List of VRH elastic moduli recommended for use in VCCTL. K = bulk modulus; G = shear modulus; E = Young’s modulus; ν = Poisson’s ratio.

Phase	K (GPa)	G (GPa)	E (GPa)	ν	Reference
Alite (C_3S)	112	52	135	0.30	[24, 27, 29]
Belite (β - C_2S)	111	53	137	0.29	[24, 27, 29]
Aluminate (C_3A)	103	54	138	0.28	[24, 27, 28, 29]
Ferrite (C_4AF)	146	48	130	0.35	[24, 25, 26, 27, 29]
Gypsum	43	15	41	0.35	[33]
Bassanite	90	54	135	0.25	[35]
Anhydrite	56	30	76	0.28	[34]
Ettringite	28	10	25	0.35	[31]
Monosulfate	32	21	51	0.23	Assumed (see text)
C–S–H	29	13	34	0.31	This study
Portlandite (CH)	32	21	51	0.23	[32]
Calcite	76	33	86	0.32	[30]

drated cement binder materials. Therefore, any error associated with the intrinsic properties of C–S–H will have a significant impact on the computed effective properties of the material. Constantinides and Ulm [37] used nano indentation to obtain values for the Young’s modulus of C–S–H ranging from 18 GPa to 36 GPa. Such a large spread in the values of the measured moduli is likely the result of averaging over regions of C–S–H particles, characterized by a nanometer length scale, due to the spatial resolution of the nano-indenter ($\sim 1 \mu\text{m}$). Simulations performed using semi-empirical force fields [38] gave values of $K = 51$ GPa, $G = 22$ GPa, $E = 58$ GPa, and $\nu = 0.31$ for a stoichiometry $C_{1.65}SH_{1.75}$, which accounts for structural water but not liquid water in the gel porosity. Here, the elastic properties of saturated C–S–H are needed, since all the experimental measurements and simulations are performed in saturated conditions. A stoichiometry $C_{1.7}SH_4$, which accounts for adsorbed water and liquid water trapped within the gel porosity, is assumed for saturated C–S–H gel [39].

In the absence of experimental measurements or calculations on saturated C–S–H gel, we estimate the elastic properties of water-saturated C–S–H using a two-phase system that consists of two end members, namely $C_{1.65}SH_{1.75}$ (“dry” C–S–H) and H_2O . The dry C–S–H end member is assigned the above elastic properties calculated by Shahsavari [38] and a density of 2600 kg/m^3

as determined by Allen et al. [40] using small angle scattering measurements for a similar stoichiometry. Water is assigned a bulk modulus $K_w = 2.2$ GPa, a shear modulus $G_w = 0$ GPa [5], and a density of $\rho_w = 1000$ kg/m³. We assume that the bulk modulus of the water-saturated form of C–S–H can be written as a linear combination of the bulk moduli of the end members:

$$\begin{aligned} K_{\text{sat}} &= xK_{\text{dry}} + (1 - x)K_w \\ &= 2.2 + 48.8x \text{ (GPa)} \end{aligned} \quad (2)$$

The unknown x is determined by enforcing the same linear relation on the density of water-saturated C–S–H, which is assumed in advance to be 1900 kg/m³ based on values reported for saturated pastes [39]:

$$1900 = 1000 + 1600x \text{ (kg/m}^3\text{)},$$

from which $x = 0.56$. Therefore, (2) gives $K_{\text{sat}} = 29$ GPa. Using the same procedure, the estimated shear modulus of water-saturated C–S–H is $G_{\text{sat}} = 13$ GPa. The remaining elastic moduli can then be calculated from $(K_{\text{sat}}, G_{\text{sat}})$, resulting in an estimated Young’s modulus $E_{\text{sat}} = 34$ GPa (equal to the value previously reported in [41]) and a Poisson ratio $\nu_{\text{sat}} = 0.31$. These values are in the range of those measured by nanoindentation [37], are close to previously reported values [41, 42] and are reasonably similar to those of the other hydration products.

3.3. Cement paste and mortar simulations

A set of virtual microstructures was created, based on the material properties and mixture proportions described in Section 2. Input to VCCTL consisted of a) the dry cement clinker phase volume fractions and surface area fractions obtained by quantitative XRD and microscopy, b) the cement particle size distribution measured by laser scattering, c) the density, elastic moduli and grading of the fine aggregate, d) heat release curves obtained by isothermal calorimetry.

Two cement paste microstructures were created: 1) C2 with $w/c = 0.6$ and 2) C1 with $w/c = 0.5$. Hydration of both microstructures was simulated by VCCTL, using a constant temperature of 23 °C and 25 °C respectively, corresponding to the hydration conditions used for the in-situ XRD analyses. This represents a first level of validation, by which the consistency of

the simulated hydration kinetics is checked against the experimental measurements, by comparing the time evolution of the fraction of cement phases present in the system during the first 24 hours of hydration. A set of seven virtual mortars were then created, with proportions sand:cement:water being those of the samples used for the experimental determination of the elastic and mechanical properties (see Section 2.1) and 4 vol% of entrained air. The simulated volume is a region of interest at the scale of the cement paste ($100 \times 100 \times 100$ voxels with a resolution of $1 \mu\text{m}$ per voxel) consisting of bulk paste and interfacial transition zone (ITZ). The latter is simulated by inserting an imaginary yz -planar boundary within the microstructure that no cement particle is allowed to cross when being randomly placed. This boundary therefore acts as a physical wall constraining the local packing of cement particles, much as a physical aggregate surface does [43]. Previous studies have indicated that the ITZ thickness is approximately equal to the median cement particle size [43], and that assumption is used here as well. The simulated hydration process was performed at $20 \text{ }^\circ\text{C}$ for 28 days. The resulting microstructures were then used as input for the FE module, which calculates the elastic moduli for the bulk paste and ITZ, based on the time-dependent phase composition and spatial arrangement, using the intrinsic elastic properties displayed in Table 4. Finally, the calculated elastic moduli of bulk paste and ITZ are passed to the differential effective medium theory algorithm, which computes the elastic moduli and mechanical strength of the mortars, based on the amount, grading and intrinsic elastic properties of the sand aggregate.

4. Results

4.1. Hydration kinetics

Figure 3 compares the simulated and measured time-dependent volume fractions of the phases present in C1 and C2 pastes, hydrated at $25 \text{ }^\circ\text{C}$ and $23 \text{ }^\circ\text{C}$ respectively. The volume fractions are scaled to the total volume of the system (*i.e.*, phases and pore solution). Alite is the most abundant clinker phase, and C–S–H portlandite and ettringite are the main hydration products. Also, capillary porosity represents a fundamental microstructural feature in terms of development of mechanical properties. The experimentally measured values of the other clinker phases do not vary monotonically in time and have relatively large associated uncertainty [11]. Therefore, we

deem the hydration of these other clinker phases to be unreliable for comparing with the simulated data. The experimental volume fraction of C–S–H is estimated based on mass balance calculations [44].

The results displayed in Figure 3 show that the predicted volume fractions of alite, C–S–H, portlandite and capillary porosity generally agree with experimental measurement to within about 5 % for both cement pastes. The exception is ettringite, for which the simulations tend to underestimate the experimentally measured amounts. In particular, the experimentally determined ettringite phase fraction for C2 displays a somewhat scattered trend, which is still increasing at the end of the experiment (~ 20 h) whereas a steady state concentration of approximately 2 vol% is reached after about 10 h of simulated hydration. C1 displays a higher amount of ettringite and in this case, both the experimental and predicted volume fractions reach a steady state, although in the simulation this occurs ~ 5 h prior to what observed experimentally, with the amount of ettringite present in the system at steady state being about 20 % smaller. The lack of a steady state, as experimentally observed for C2, is likely due to the presence of a significant amount of calcite in the system, which tends to stabilize ettringite with respect to monosulfoaluminate, due to precipitation of monocarboaluminate [45, 46].

4.2. Elastic and mechanical properties

The experimental measurements of the elastic moduli and compressive strengths are reported in Table 4.

A linear relation is observed between the “dynamic” and “static” elastic moduli, with the value of the latter always being smaller compared to the dynamic modulus (see Figure 4). This behaviour is commonly observed and attributed to the non-linear nature of the stress-strain curve for cement materials, due to inelastic contributions.

Since the FE method for the computation of the elastic properties, as implemented in VCCTL, simulates the elastic response of the material, the calculated Young’s modulus is compared to the dynamic Young’s modulus. In addition, it is important to compare the experimentally determined compressive strength with that estimated by VCCTL using the empirical power-law relation, since this property is important in practical applications. As already explained in Section 3.1, an empirical power law curve is used to estimate the mortar compressive strength from the dynamic Young’s modulus. Experimental data relating the elastic moduli and compressive strength of

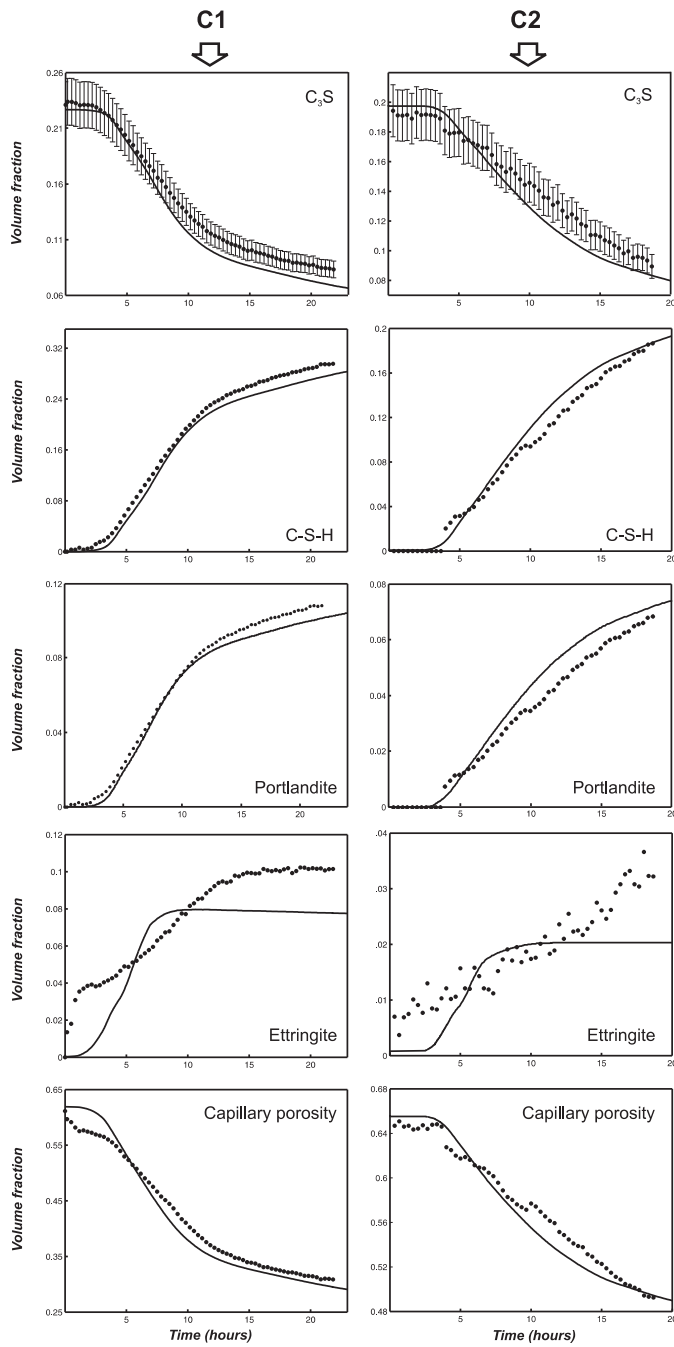


Figure 3: Variation with time of the volume fractions of alite (C_3S), C-S-H, portlandite, ettringite and capillary porosity, as measured experimentally by X-ray diffraction (circles) and simulated by VCCTL (line). The error bars for C_3S correspond to a relative error of 9 % [11].

Table 4: Summary of the experimentally measured compressive strengths and Young’s moduli for C1, C2 and C3 mortars. σ is the compressive strength. E_d and E_s are the dynamic and static compressive strength, respectively. All the values in the dataset are the average of four different measurements, with an associated uncertainty of about 10 %.

Mortar	Time (days)	σ (MPa)	E_d (GPa)	E_s (GPa)
C1 w/c 0.5	1	29.45	30.44	22.44
	7	54.02	38.16	32.04
	28	64.07	41.66	34.77
C1 w/c 0.6	1	18.35	23.52	13.89
	7	39.44	33.11	25.65
	28	48.67	36.49	28.11
C2 w/c 0.5	1	13.87	26.00	18.64
	7	38.68	35.54	29.17
	28	46.16	38.74	29.89
C2 w/c 0.55	1	10.85	22.19	15.46
	7	32.84	33.28	25.93
	28	39.85	36.38	27.98
C2 w/c 0.6	1	7.35	18.72	12.86
	7	28.14	30.48	23.45
	28	35.70	33.27	25.02
C3 + 5% SF w/c 0.5	28	63.15	-	-
	60	68.26	-	-
C3 + 10% SF w/c 0.5	28	67.64	-	-
	60	67.85	-	-

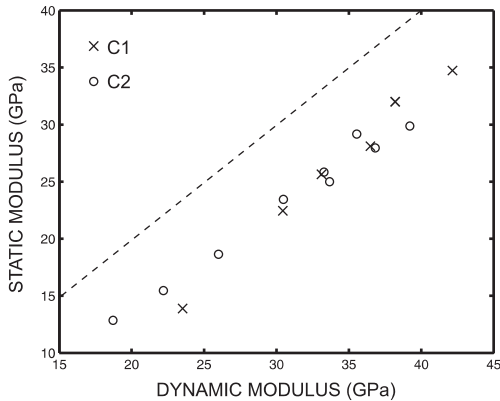


Figure 4: Plot of static vs. dynamic Young’s moduli, experimentally measured for C1 and C2 mortars. The dashed line is the line along which points with equal static and dynamic moduli would lie.

different concrete materials typically have a high amount of scatter. Therefore, using an empirical equation to represent a correlation between elastic moduli and strength therefore may adequately reflect the average correlations among such data but will have significant uncertainty when applied to a given mortar [47]. Recognizing that any such regression is empirical in nature, we opt to use a power law to estimate the compressive strength from Young’s modulus using experimental measurements on mortars using either C1 or C2 over a wide range of strength values and obtained with mixes at different ages and different w/c ratios. Furthermore, recently reported data using three different cements and a different fine aggregate [8], are also used in the calibration to widen the scope of materials and range of validity of the relation. Based on these data, shown in Figure 5, the best two-parameter power law fit, with a coefficient of determination $R^2 = 0.9945$, is

$$\sigma \text{ (MPa)} = 3.79 \times 10^{-3} E \text{ (GPa)}^{2.60} \quad (3)$$

We wish to emphasize the empirical nature of this equation; one should be cautious about applying the same power law to a mortar that is much different in nature from the ones used in the regression. Here, in order to give an estimate of the error associated to the use of this relation, compressive strengths are calculated for the mix C3, which is not included in the dataset displayed in Figure 5.

Measured and calculated values of Young’s moduli and compressive strength at different ages and w/c, for C1, C2 and C3, are displayed in Figure 6–8.

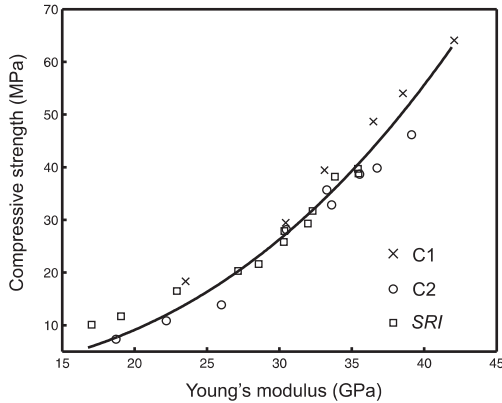


Figure 5: Plot of compressive strength vs. Young's modulus, experimentally measured for mortars made with C1 and C2, and taken from mortar data obtained by SRI [8]. The curve is the power-law regression for all of the data (see 3).

Again, very good agreement between simulation and experiment is observed both for the moduli and the compressive strengths, for all mixes, at the different hydration times, w/c and silica fume additions considered. In fact, the predicted moduli and strengths generally lie within the 10 % coefficient of variation in the measured values.

5. Discussion and conclusions

In this study, we have shown the ability of the microstructural model VCCTL as a tool for the design of cementitious materials. VCCTL takes as input the following experimental data:

1. cement phase composition;
2. particle size distribution and shape;
3. w/c ratio;
4. heat release curve;
5. aggregate grading, density and elastic moduli.

The output returned by VCCTL consists of the virtual 3D microstructure, time-dependent phase composition and elastic moduli of the simulated material. The elastic moduli of the mortars are calculated by the model from the simulated 3D microstructure. Since there is no physical theory that directly links the elastic moduli to mechanical properties such as compressive

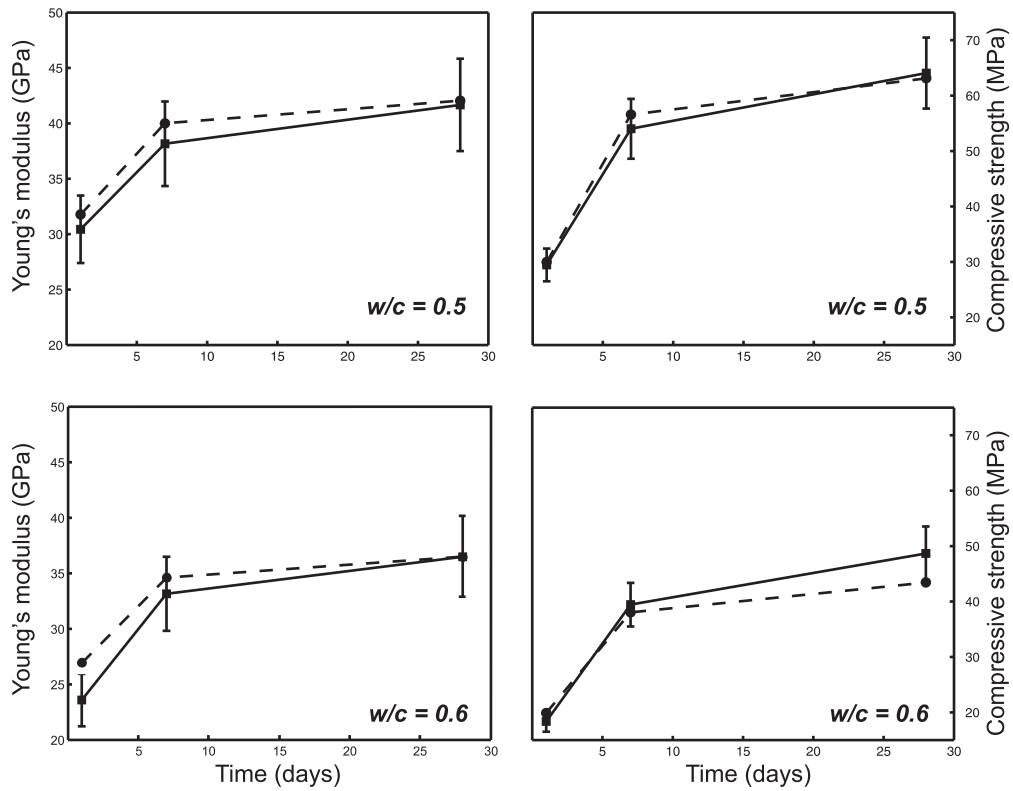


Figure 6: Plots of Young's modulus and compressive strength versus time, as experimentally measured (squares) and simulated (circles) for C1 mortars at different values of w/c . The vertical lines mark a 10 % coefficient of variation. The solid and dashed lines connecting the points are provided as a visual aid only.

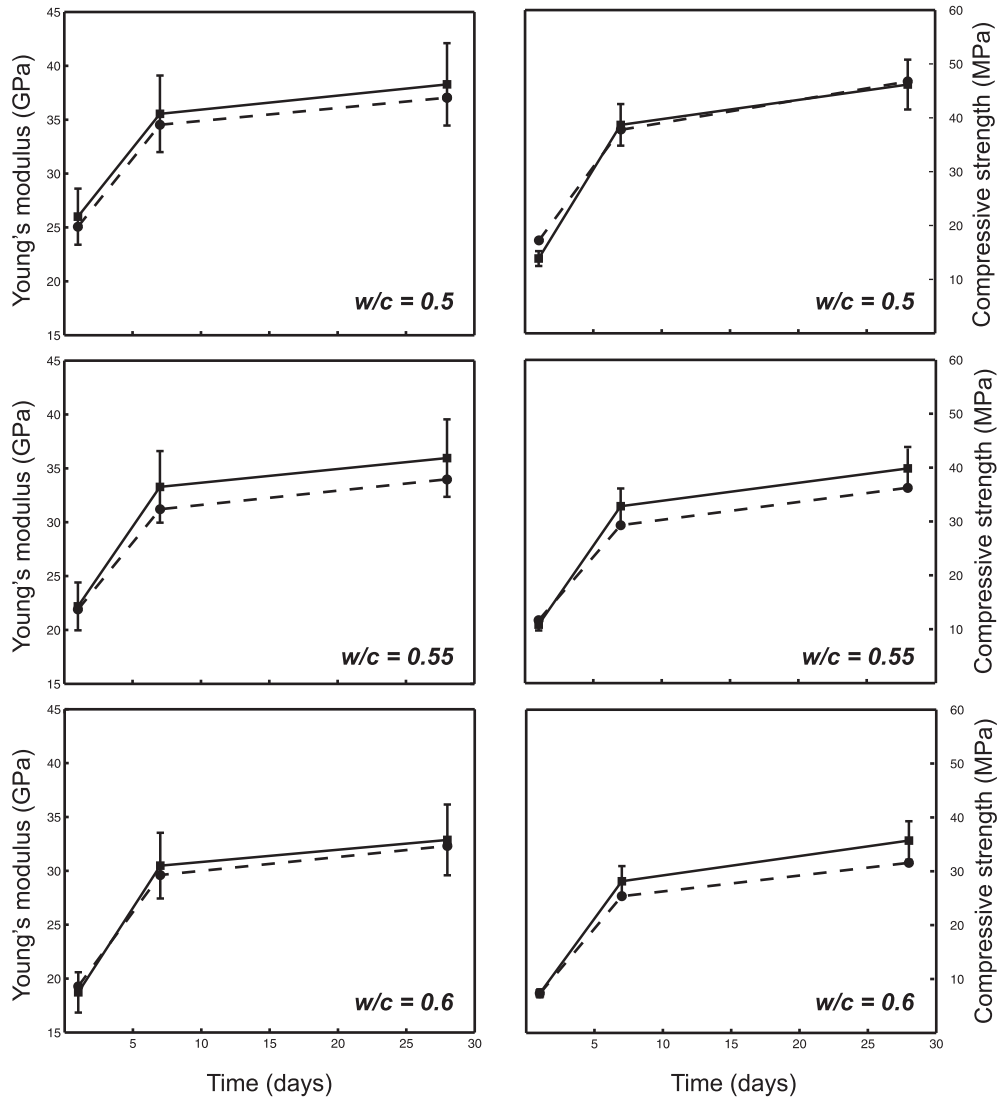


Figure 7: Plots of Young's modulus and compressive strength versus time, as experimentally measured (squares) and simulated (circles) for C2 mortars at different values of w/c. The vertical lines mark a 10 % coefficient of variation. The solid and dashed lines connecting the points are provided as a visual aid only.

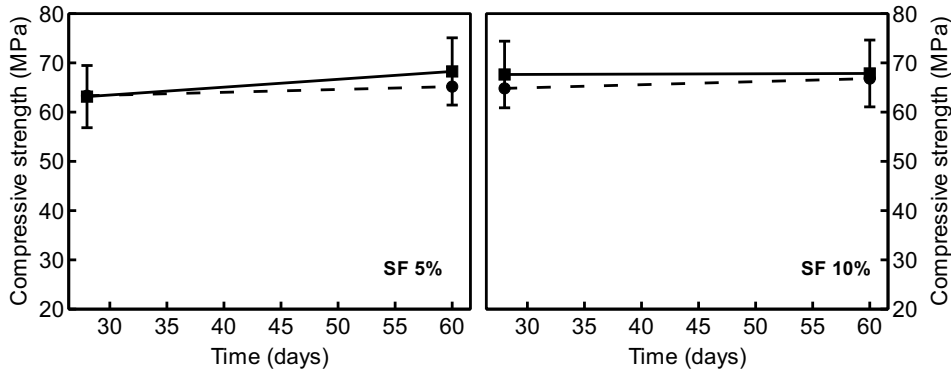


Figure 8: Plots of compressive strengths versus time, as experimentally measured (squares) and simulated (circles) for C3 mortars, having 5% and 10% silica fume. The vertical lines mark a 10 % coefficient of variation. The solid and dashed lines connecting the points are provided as a visual aid only.

strength, the latter has to be estimated using experimental calibration curves that relate the two physical quantities.

One of the novel aspects of this study, compared to previous applications of microstructural models, is that the simulated early age hydration kinetics of the individual phases is compared to the real kinetics obtained by in-situ XRD experimental measurements. The results (Figure 3) show that VCCTL captures, to a very good approximation, the time variation of the volume fraction of C-S-H, portlandite and capillary porosity, which are the main constituents that determine the final elastic and mechanical properties of the material. The time variation of the volume fraction of alite, the main clinker phase, is also appropriately reproduced by the model, with the differences between experimental observations and simulations mostly lying within the extent of the experimental uncertainties. On the contrary, more significant differences are observed for the curves describing the time evolution of ettringite. However, given the relatively small amounts of ettringite present in the system, the observed differences, of less than 3 % of the total volume of the system, are not likely to have a significant effect on the physical properties of the material as a whole.

The results outlined in Section 4.2 and displayed in Figures 6–8 show a very good agreement between the measured and predicted dynamic Young’s moduli and compressive strengths. The results also show that the Young’s moduli can be converted to compressive strength, by using the power law

relation displayed in Equation 3, with very accurate results for both the cements used for the calibration of the “compressive strength vs. Young’s modulus” and the cement blended with different amounts of silica fume, which had not been used for the calibration.

In conclusion, VCCTL proved to adequately predict both the early age hydration kinetics and the elastic properties of mortars obtained from different cements. Empirical relations can be used to estimate the compressive strength of the virtual materials with good accuracy.

Acknowledgements

This work was performed within the framework of the MAPEI-UNIPD research agreement. Wilasa Vichit-Vadakan of Siam Research and Innovation Co., Ltd. is acknowledged for providing elastic moduli and compressive strength data. André Nonat and Ed Garboczi are gratefully acknowledged for insightful comments on an earlier version of the manuscript. Two anonymous reviewers are thanked for their suggestions, which greatly improved the quality of the manuscript. John Bolander is acknowledged for editorial handling.

References

- [1] Z. Sun, E. J. Garboczi, S. P. Shah, Modeling the elastic properties of concrete composites: Experiment, differential effective medium theory, and numerical simulation, *Cem. Concr. Compos.* 29 (1) (2007) 22 – 38.
- [2] J. W. Bullard, P. E. Stutzman, Analysis of ccr1 proficiency cements 151 and 152 using the Virtual Cement and Concrete Testing Laboratory, *Cem. Concr. Res.* 36 (8) (2006) 1548 – 1555.
- [3] J. W. Bullard, E. J. Garboczi, A model investigation of the influence of particle shape on portland cement hydration, *Cem. Concr. Res.* 36 (6) (2006) 1007 – 1015.
- [4] D. P. Bentz, Three-dimensional computer simulation of portland cement hydration and microstructure development, *J. Am. Ceram. Soc.* 80 (1) (1997) 3–21.

- [5] C.-J. Haecker, E. J. Garboczi, J. W. Bullard, R. B. Bohn, Z. Sun, S. P. Shah, T. Voigt, Modeling the linear elastic properties of portland cement paste, *Cem. Concr. Res.* 35 (10) (2005) 1948 – 1960.
- [6] V. Smilauer, Z. Bittnar, Microstructure-based micromechanical prediction of elastic properties in hydrating cement paste, *Cem. Concr. Res.* 36 (9) (2006) 1708 – 1718.
- [7] L. Stefan, F. Benboudjema, J.-M. Torrenti, B. Bissonnette, Prediction of elastic properties of cement pastes at early ages, *Comput. Mater. Sci.* 47 (3) (2010) 775 – 784.
- [8] P. Sahachaiyunta, K. Pongpaisanseree, J. W. Bullard, P. E. Stutzman, E. J. Garboczi, W. Vichit-Vadakan, Virtual testing in a cement plant, *Concr. Int.* 34 (9) (2012) 33 – 39.
- [9] DIN EN 197-1. Composition, specifications and conformity criteria for common cements, Tech. rep., CEN European Committee for Standardization (August 2004).
- [10] DIN EN 196-1. Methods of testing cement—Part 1: Determination of strength, Tech. rep., CEN European Committee for Standardization (May 2005).
- [11] L. Leon-Reina, A. G. De la Torre, J. M. Porras-Vazquez, M. Cruz, L. M. Ordonez, X. Alcobe, F. Gispert-Guirado, A. Larranaga-Varga, M. Paul, T. Fuellmann, R. Schmidt, M. A. G. Aranda, Round robin on Rietveld quantitative phase analysis of Portland cements, *J. Appl. Cryst.* 42 (5) (2009) 906–916.
- [12] UNI 6556. Tests of concretes. determination of static modulus of elasticity in compression, Tech. rep., UNI: Ente Nazionale Italiano di Unificazione (March 1976).
- [13] R. W. Cheary, A. A. Coelho, J. P. Cline, Fundamental parameters line profile fitting in laboratory diffractometers, *J. Res. Natl. Inst. Stand. Technol.* 109 (2004) 1 – 25.
- [14] Crystallographic databases, www.nist.gov/mml/mmsd/structure_determination/crystallographic-databases.cfm.

- [15] C. Hesse, F. Goetz-Neunhoeffer, J. Neubauer, M. Braeu, P. Gaebel-
lein, Quantitative in situ x-ray diffraction analysis of early hydration of
portland cement at defined temperatures, *Powder Diffr.* 24 (02) (2009)
112–115.
- [16] L. Valentini, M. C. Dalconi, M. Parisatto, G. Cruciani, G. Artioli,
Towards three-dimensional quantitative reconstruction of cement mi-
crostructure by x-ray diffraction microtomography, *J. Appl. Crystallogr.*
44 (2) (2011) 272–280.
- [17] E. J. Garboczi, J. W. Bullard, Shape analysis of a reference cement,
Cem. Concr. Res. 34 (10) (2004) 1933 – 1937.
- [18] E. J. Garboczi, Three-dimensional mathematical analysis of particle
shape using x-ray tomography and spherical harmonics: Application
to aggregates used in concrete, *Cem. Concr. Res.* 32 (10) (2002) 1621 –
1638.
- [19] D. P. Bentz, Quantitative comparison of real and CEMHYD3D model
microstructures using correlation functions, *Cem. Concr. Res.* 36 (2)
(2006) 259 – 263.
- [20] E. J. Garboczi, A. R. Day, An algorithm for computing the effective
linear elastic properties of heterogeneous materials: Three-dimensional
results for composites with equal phase poisson ratios, *J. Mech. Phys.*
Solids 43 (9) (1995) 1349 – 1362.
- [21] E. J. Garboczi, J. G. Berryman, Elastic moduli of a material contain-
ing composite inclusions: effective medium theory and finite element
computations, *Mech. Mater.* 33 (8) (2001) 455 – 470.
- [22] A. M. Neville, *Properties of Concrete*, Prentice-Hall, Harlow, England,
1995.
- [23] R. J. Angel, J. M. Jackson, H. J. Reichmann, S. Speziale, Elasticity
measurements on minerals: a review, *Eur. J. Mineral.* 21 (3) (2009)
525–550.
- [24] K. Velez, S. Maximilien, D. Damidot, G. Fantozzi, F. Sorrentino, Deter-
mination by nanoindentation of elastic modulus and hardness of pure

- constituents of portland cement clinker, *Cem. Concr. Res.* 31 (4) (2001) 555 – 561.
- [25] N. L. Ross, R. J. Angel, F. Seifert, Compressibility of brownmillerite ($\text{Ca}_2\text{Fe}_2\text{O}_5$): effect of vacancies on the elastic properties of perovskites, *Phys. Earth Planet. Inter.* 129 (12) (2002) 145 – 151.
- [26] C. Vanpeteghem, R. Angel, J. Zhao, N. Ross, G. Redhammer, F. Seifert, The effect of oxygen vacancies and aluminium substitution on the high-pressure properties of brownmillerite-structured $\text{Ca}_2\text{Fe}_{2-x}\text{Al}_x\text{O}_5$, *Phys. Chem. Miner.* 35 (2008) 493–504.
- [27] V. Swamy, L. S. Dubrovinsky, Thermodynamic data for the phases in the CaSiO_3 system, *Geochim. Cosmochim. Acta* 61 (6) (1997) 1181 – 1191.
- [28] H. Manzano, J. S. Dolado, A. Ayuela, Structural, mechanical, and reactivity properties of tricalcium aluminate using first-principles calculations, *J. Am. Ceram. Soc.* 92 (4) (2009) 897–902.
- [29] H. Manzano, J. S. Dolado, A. Ayuela, Elastic properties of the main species present in Portland cement pastes, *Acta Mater.* 57 (5) (2009) 1666 – 1674.
- [30] C.-C. Chen, C.-C. Lin, L.-G. Liu, S. V. Sinogeikin, J. D. Bass, Elasticity of single-crystal calcite and rhodochrosite by Brillouin spectroscopy, *Am. Min.* 86 (11-12) (2001) 1525–1529.
- [31] S. Speziale, F. Jiang, Z. Mao, P. J. M. Monteiro, H.-R. Wenk, T. S. Duffy, F. R. Schilling, Single-crystal elastic constants of natural ettringite, *Cem. Concr. Res.* 38 (7) (2008) 885 – 889.
- [32] S. Speziale, H. J. Reichmann, F. R. Schilling, H. Wenk, P. J. M. Monteiro, Determination of the elastic constants of portlandite by Brillouin spectroscopy, *Cem. Concr. Res.* 38 (10) (2008) 1148 – 1153.
- [33] S. Haussuehl, Elastische und thermoelastische eigenschaften von $\text{CaSO}_4 \cdot 2\text{H}_2\text{O}$ (gips), *Z. Kristallogr.* 122 (1965) 311–314.
- [34] W. M. Schwerdtner, J. C.-M. Tou, P. B. Hertz, Elastic properties of single crystals of anhydrite, *Can. J. Earth Sci.* 2 (1965) 673–683.

- [35] P. Comodi, S. Nazzareni, L. Dubrovinsky, M. Merlini, The high-pressure–high-temperature behavior of bassanite, *Am. Min.* 94 (11-12) (2009) 1596–1602.
- [36] A. Mesbah, M. Franois, C. C. dit Coumes, F. Frizon, Y. Filinchuk, F. Leroux, J. Ravaux, G. Renaudin, Crystal structure of Kuzel’s salt $3\text{CaO}\cdot\text{Al}_2\text{O}_3\cdot 1/2\text{CaSO}_4\cdot 1/2\text{CaCl}_2\cdot 11\text{H}_2\text{O}$ determined by synchrotron powder diffraction, *Cem. Concr. Res.* 41 (5) (2011) 504 – 509.
- [37] G. Constantinides, F.-J. Ulm, The effect of two types of C–S–H on the elasticity of cement-based materials: Results from nanoindentation and micromechanical modeling, *Cem. Concr. Res.* 34 (1) (2004) 67 – 80.
- [38] R. Shahsavari, R. J.-M. Pellenq, F.-J. Ulm, Empirical force fields for complex hydrated calcio-silicate layered materials, *Phys. Chem. Chem. Phys.* 13 (2011) 1002–1011.
- [39] H. F. W. Taylor, *Cement chemistry*, Thomas Telford, London, UK, 1997.
- [40] A. J. Allen, J. J.-M. Thomas, H. H. Jennings, Composition and density of nanoscale calciumsilicatehydrate in cement, *Nat. Mater.* 6 (2007) 312 – 316.
- [41] J. J. Beaudoin, R. Feldman, J. Baron, M. Conjeaud, Dependence of degree of silica polymerization and intrinsic mechanical properties of C–S–H on C/S ratio, in: *Proc. 8th Int. Cong. Chem. Cem.*, Rio de Janeiro, Brazil, 1986.
- [42] P. Acker, Micromechanical analysis of creep and shrinkage mechanisms, in: F.-J. Ulm, Z. Bazant, F. Wittman (Eds.), *Creep, Shrinkage and Durability Mechanics of Concrete and other Quasi-Brittle Materials*, 1999.
- [43] D. P. Bentz, E. J. Garboczi, Computer modelling of interfacial transition zone: microstructure and properties, in: M. G. Alexander, G. Arliguie, G. Ballivy, A. Bentur, J. Marchand (Eds.), *Engineering and Transport Properties of the Interfacial Transition Zone in Cementitious Composites - State-of-the-Art Report of RILEM TC 159-ETC and 163-TP*, 1999.
- [44] L. Valentini, *RieCalc*: quantitative phase analysis of hydrating cement pastes, *J. Appl. Crystallogr.* 46 (6) (2013) 1899–1902.

- [45] T. Matschei, B. Lothenbach, F. P. Glasser, Thermodynamic properties of portland cement hydrates in the system $\text{CaO-Al}_2\text{O}_3\text{-SiO}_2\text{-CaSO}_4\text{-CaCO}_3\text{-H}_2\text{O}$, *Cem. Concr. Res.* 37 (10) (2007) 1379 – 1410.
- [46] J. W. Bullard, B. Lothenbach, P. E. Stutzman, K. A. Snyder, Coupling thermodynamics and digital image models to simulate hydration and microstructure development of portland cement pastes, *J. Mater. Res.* 26 (4) (2011) 609 – 622.
- [47] T. Noguchi, F. Tomosawa, K. M. Nematì, B. M. Chiaia, A. P. Fantilli, A practical equation for elastic modulus of concrete, *ACI Struct. J.* 106 (5) (2009) 690 – 696.